Channel Estimation for Extremely Large-Scale Massive MIMO Systems

Yu Han, Shi Jin, Chao-Kai Wen, and Xiaoli Ma

***Abstract*—Extremely large-scale massive multiple-input multiple-output has shown considerable potential in future mobile communications. However, the use of extremely large aperture arrays will lead to near-field and spatial non-stationary channel conditions, which result in changes in transceiver design and channel state information acquisition. This letter focuses on the channel estimation problem and describes the non-stationary channel through a mapping between subarrays and scatterers. We propose subarray-wise and scatterer-wise channel estimation methods to estimate the near-field non-stationary channel from the views of the subarray and the scatterer, respectively. Numerical results demonstrate that the subarray-wise method can derive accurate channel estimation results with low complexity, whereas the scatterer-wise method can accurately position the scatterers and identify almost all the mappings between subarrays and scatterers.**

***Index Terms*—Extremely large-scale massive MIMO, spherical wave, non-stationary, channel estimation.**

I. Introduction

EXTREMELY large-scale massive multiple-input multiple-output (MIMO) is a promising research direction for multi-antenna technology, in which a significant number of antennas can be widely spread (e.g., on the walls of dense buildings in the city) [1]. Extremely large-scale massive MIMO can produce seamless mobile communication services because users are surrounded by base station (BS) antennas. However, the use of large aperture arrays and the close distance between an array and a user will result in different channel conditions. One of the differences is *near-field propagation*. If users and scatterers are located inside the Rayleigh distance of the array, then the array will experience spherical wavefronts instead of planar wavefronts [2]–[4]. Another difference is *spatial non-stationarity* [5]–[8]. Spatial stationarity holds when the entire array has limited aperture and sees the same scatterers. However, for a large aperture array, previous channel measurement results [5] show that different regions of the array will receive varying levels of powers due to the different scatterers they can see; this condition is called spatial non-stationarity. Consequently, visibility regions (VRs) of subarrays and scatterers are introduced to describe the non-stationarity.

Under near-field non-stationary channel conditions, the transceiver should be redesigned, but such changes will raise new requirements when acquiring channel state information. Theoretical analysis found that the signal-to-interference-and-noise ratio of each user increases if the VRs of different users do not overlap [6]. Therefore, low-complexity subarray-based transceivers can be designed with the knowledge of the VRs [5]–[7]. If the positions of the scatterers can be further obtained, then enhanced transceiver designs will be enabled. Traditional channel estimation methods, such as least squares (LS) and linear minimum mean square error [9], cannot satisfy the above requirements. Although numerous studies have been conducted on the positioning scatterers in near-field stationary channels [3], [4], and some research has begun to focus on the estimation of VRs of scatterers [8], only a few studies are available on the positioning of scatterers simultaneous with the identification of VRs.

This letter proposes a subarray-wise channel estimation method and a scatterer-wise method to explore the near-field non-stationary channel. We model the multipath channel with the last-hop scatterers under a spherical wavefront and divide the large aperture array into multiple subarrays. Given the stationarity in each subarray, the subarray-wise method treats one subarray individually and positions the visible scatterers of each subarray based on a refined orthogonal matching pursuit (OMP) algorithm. The array gain integrated by multiple subarrays is utilized, then the scatterer-wise method simultaneously positions each scatterer and detects its VR to further enhance the positioning accuracy. Numerical results demonstrate that the subarray-wise method can achieve an excellent mean square error (MSE) performance with low complexity, whereas the scatterer-wise method can accurately position the scatterers and determine the non-stationary channel.

II. System Model

In an extremely large-scale massive MIMO system, the BS is equipped with an M-element uniform linear array (ULA),[1] where M can be 10^3 or larger. The distance between two adjacent ULA elements is d. Note that distances and coordinates are normalized by the carrier wavelength in this letter. The ULA center serves as the origin of an xy coordinate system, as shown in Fig. 1(a). The ULA lies along the y-axis. The coordinate of ULA element m is $(0, (m-1-\frac{M-1}{2})d)$, where

Manuscript received October 10, 2019; revised December 15, 2019; accepted December 26, 2019. Date of publication January 3, 2020; date of current version May 8, 2020. The work of Yu Han and Shi Jin was supported in part by the National Science Foundation of China (NSFC) for Distinguished Young Scholars of China under Grant 61625106, in part by NSFC under Grant 61921004, in part by the Scholarship from the China Scholarship Council under Grant 201806090062, and in part by the Scientific Research Foundation of Graduate School of Southeast University under Grant YBPY1860. The work of Chao-Kai Wen was supported in part by the Ministry of Science and Technology of Taiwan under Grant MOST 108-2628-E-110-001-MY3, and in part by the ITRI in Hsinchu, Taiwan. The associate editor coordinating the review of this article and approving it for publication was H. Q. Ngo. *(Corresponding author: Shi Jin.)*

Yu Han and Shi Jin are with the National Mobile Communications Research Laboratory, Southeast University, Nanjing 210096, China (e-mail: hanyu@seu.edu.cn; jinshi@seu.edu.cn).

Chao-Kai Wen is with the Institute of Communications Engineering, National Sun Yat-sen University, Kaohsiung 80424, Taiwan (e-mail: chaokai.wen@mail.nsysu.edu.tw).

Xiaoli Ma is with the School of Electrical and Computer Engineering, Georgia Institute of Technology, Atlanta, GA 30332 USA (e-mail: xiaoli@gatech.edu).

Digital Object Identifier 10.1109/LWC.2019.2963877

[1]ULA is reduced from the more widely used uniform planar array (UPA). Channel estimation methods proposed in this letter can be easily extended to UPA cases, where three-dimensional coordinate system should be considered.

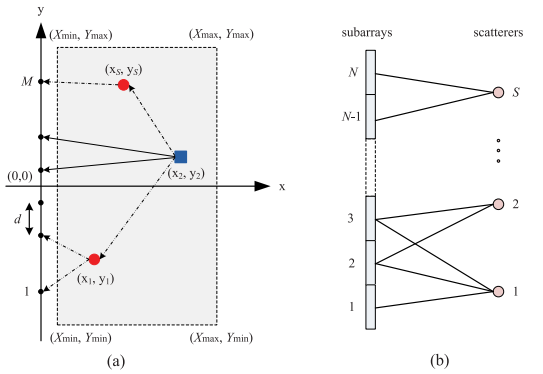

Fig. 1. Extremely large-scale massive MIMO. (a) ULA elements (black dots), user (blue square), and scatterers (red circles) in the *xy* coordinate system. (b) Mapping between subarrays and scatterers (including the user antenna).

$m = 1, \ldots, M$. To describe the spatial non-stationary channel, we uniformly divide the ULA into *N* subarrays, each with *M/N* antennas. If *M/N* is small, then each subarray is regarded to experience spatial stationarity.

Users are located in the positive *x*-axis region, and a certain single-antenna user is considered accordingly.[2] As shown in Fig. 1(a), the signal sent by the user may arrive at the ULA along the line-of-sight (LoS) path or be reflected by multiple scatterers. We only focus on the last-jump scatterers of the paths in the VR of the ULA. User antenna is set to be equivalent to the scatterer for the LoS path. The coordinate of the scatterer *s* is denoted by (x_s, y_s) to satisfy $X_{\min} < x_s < X_{\max}$, $Y_{\min} < y_s < Y_{\max}$; *S* is the number of scatterers (including the user antenna); and $X_{\min}$, $X_{\max}$, $Y_{\min}$, and $Y_{\max}$ represent the bounds of the VR of the ULA.

1) *Near-field property:* The wireless signal has a spherical wavefront. The array response stimulated by the scatterer at (*x*, *y*) is denoted by $\mathbf{a}(x, y) \in \mathbb{C}^{M\times 1}$, whose *m*th entry is [2]:

$$[\mathbf{a}(x, y)]_m = \frac{D_o(x, y)}{D_m(x, y)} e^{j2\pi D_m(x,y)}, \tag{1}$$

where $D_o(x, y) = x$ is the distance between the scatterer and the ULA. In addition,

$$D_m(x, y) = \sqrt{x^2 + (y - d(m - (M + 1)/2))^2} \tag{2}$$

is the distance between the scatterer and the ULA element *m*, where $m = 1, \ldots, M$.

2) *Spatial non-stationarity:* Different subarrays see different scatterers and vice versa. Subarray *n* can receive signals reflected by scatterers (i.e., the VR of subarray *n*):

$$\Psi_n = \{s_{n,1}, \ldots, s_{n,S_n}\}, \tag{3}$$

which satisfies $1 \le s_{n,i} \le S$ and $0 \le S_n \le S$. Similarly, scatterer *s* can see subarrays (i.e., the VR of subarray *n*):

$$\Phi_s = \{n_{s,1}, \ldots, n_{s,N_s}\}, \tag{4}$$

which satisfies $1 \le n_{s,j} \le N$ and $1 \le N_s \le N$. In the above expressions, Ψ_n and Φ_s describe the mapping between subarrays and scatterers from their corresponding views. On the basis of the mapping in Fig. 1 (b), we can obtain $\Psi_1 = \{1\}$, $\Psi_2 = \Psi_3 = \{1, 2\}$, $\Psi_{N-1} = \Psi_N = \{S\}$, and $\Phi_1 = \{1, 2, 3\}$, $\Phi_2 = \{2, 3\}$, $\Phi_S = \{N - 1, N\}$.

Given the two properties, we model the multipath channel from the user to the BS as

[2]Channel estimations of different users are identical and independent from each other. Therefore, we consider the estimation of a single user channel.

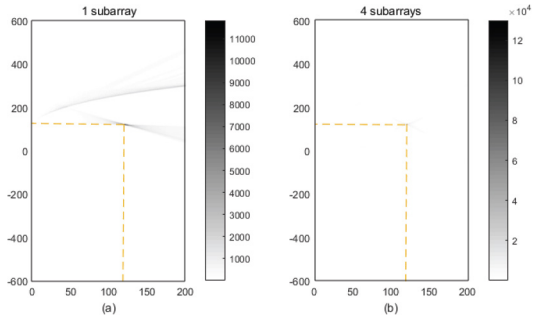

Fig. 2. Array pattern of a ULA when (a) one subarray and (b) four subarrays can see the scatterer at (120, 120).

$$\mathbf{h} = \sum_{s=1}^{S} g_s \mathbf{a}(x_s, y_s) \odot \mathbf{p}(\Phi_s), \tag{5}$$

where g_s is the complex attenuation factor of path *s*, (x_s, y_s) is the coordinate of the *s*th last-hop scatterer, $\odot$ denotes Hadamard product, $\mathbf{p}(\Phi_s) \in \mathbb{Z}^{M\times 1}$ selects the subarrays that can see the *s*th scatterer with the *m*th entry to be

$$[\mathbf{p}(\Phi)]_m = \begin{cases} 1, & \text{if } \lceil \frac{mN}{M} \rceil \in \Phi, \\ 0, & \text{else}, \end{cases} \tag{6}$$

and $\lceil \cdot \rceil$ rounds a decimal to its nearest higher integer.

During the channel estimation phase, the user sends all-1 pilots to the BS. The pilot received by the BS is denoted by $\mathbf{r} = \sqrt{P}\mathbf{h} + \mathbf{w}$, where *P* is the transmitted power, and $\mathbf{w} \in \mathbb{C}^{M\times 1}$ is the additive Gaussian noise with zero means and unit variance. Given $\mathbf{r}$, the BS then estimates channel $\mathbf{h}$, and more importantly, obtains (x_s, y_s) and Ψ_n or Φ_s for the subsequent transceiver design or other applications.

III. Channel Estimation Methods

In this section, we develop two methods to estimate the near-field non-stationary channel. We also identify the positions of the scatterers and determine the mapping from the views of the subarray and the scatterer, respectively.

A. Array Pattern

In traditional far-field stationary massive MIMO systems, when the number of paths is incomparable to the number of antennas, the channel is in sparsity state in the angular domain and we can extract the paths. This sparsity is partially a result of the directionality of the array pattern. If the array pattern of the extremely large-scale massive MIMO system still holds directionality, then we can reuse the methods designed for massive MIMO systems to estimate the near-field non-stationary channel.

We define the radiation power from the signal $\mathbf{z} \in \mathbb{C}^{M\times 1}$ to the (*x*, *y*)-direction when subarrays in Φ receive $\mathbf{z}$ as

$$\rho_{\Phi,\mathbf{z}\to(x,y)} = \left|(\mathbf{z} \odot \mathbf{p}(\Phi))^H \mathbf{b}(x, y)\right|^2, \tag{7}$$

where $[\mathbf{b}(x, y)]_m = e^{j2\pi D_m(x,y)}$. The array pattern is obtained by calculating the radiation power from $\mathbf{z} = \mathbf{a}(x_s, y_s)$ to all sampled directions that cover the VR of the ULA:

$$\Xi = \{(x, y) | x = X_{\min}, X_{\min} + \Delta x, \ldots, X_{\max}; \\ y = Y_{\min}, Y_{\min} + \Delta y, \ldots, Y_{\max}\}, \tag{8}$$

where Δx and Δy are the step lengths on the *x*- and *y*-axes, respectively. Fig. 2 shows the patterns of the 1,024-element ULA, where $N = 8$, $d = 1/2$, $X_{\min} = 0$, $X_{\max} = 200$, $Y_{\min} = -600$, $Y_{\max} = 600$, $\Delta x = \Delta y = 1$, $x_s = y_s = 120$,

and (a) $\Phi_s = \{4\}$, (b) $\Phi_s = \{2, 3, 4, 5\}$. Despite the different sizes of Φ_s, the strongest radiation power appears exactly at the target position and is considerably larger than the radiation power of other positions, demonstrating the directionality of the array pattern and the sparsity of the channel[3] under the near-field non-stationary condition. Therefore, sparse signal recovery algorithms, such as OMP [10], can be applied to extract the paths from the noisy mixture $\mathbf{r}$. The channel estimation problem is translated to

$$\begin{aligned} \min_{(x_s,y_s),\Phi_s,g_s} \quad & \left\| \mathbf{r} - \sqrt{P} \sum_{s=1}^{S} g_s \mathbf{a}(x_s, y_s) \odot \mathbf{p}(\Phi_s) \right\|^2, \\ \text{s.t.} \quad & (x_s, y_s) \in \Xi \quad \text{and} \quad \Phi_s \neq \emptyset. \end{aligned} \tag{9}$$

B. Subarray-Wise Channel Estimation

A subarray is the smallest unit experiencing stationarity. The subchannel on subarray *n* is

$$\mathbf{h}_n = \sum_{s \in \Psi_n} g_s \mathbf{a}_n(x_s, y_s), \tag{10}$$

where $\mathbf{a}_n(x, y) \in \mathbb{C}^{\frac{M}{N} \times 1}$ is the *n*th subvector of $\mathbf{a}(x, y)$. If low-complexity subarray-based transceiver designs for traditional stationary systems are adopted, then each subarray is treated individually. In this case, the subarray-wise method is proposed to estimate $\mathbf{h}_n$ from $\mathbf{r}_n = \sqrt{P}\mathbf{h}_n + \mathbf{w}_n$, where $\mathbf{r}_n, \mathbf{w}_n \in \mathbb{C}^{\frac{M}{N} \times 1}$ represent the *n*th subvectors of $\mathbf{r}$ and $\mathbf{w}$, respectively.

OMP is an iterative algorithm performed in a greedy manner. When applied to a channel estimation problem, OMP extracts only one path within each iteration. At the end of the $(s-1)$st iteration, $s-1$ paths are supposedly extracted from $\mathbf{r}_n$, and the residue is given as:

$$\mathbf{r}_{n,\text{res}}^{(s)} = \mathbf{r}_n - \sqrt{P} \sum_{i=1}^{s-1} \tilde{g}_{n,i} \mathbf{a}_n(\tilde{x}_{n,i}, \tilde{y}_{n,i}), \tag{11}$$

where $\tilde{g}_{n,i}$ and $(\tilde{x}_{n,i}, \tilde{y}_{n,i})$ are the estimates of $g_{s_{n,i}}$ and $(x_{s_{n,i}}, y_{s_{n,i}})$, respectively. In the *s*th iteration, path *s* is extracted by calculating $\tilde{g}_{n,s}$ and $(\tilde{x}_{n,s}, \tilde{y}_{n,s})$ from $\mathbf{r}_{n,\text{res}}^{(s)}$ to minimize the residue power.

Coordinate $(\tilde{x}_{n,s}, \tilde{y}_{n,s})$ is obtained from grid Ξ. In view of the on-grid effect, Ξ should be a dense grid to guarantee the accuracy of $(\tilde{x}_{n,s}, \tilde{y}_{n,s})$. However, the exhaustive search for a dense grid is time-consuming. Thus, we refine the OMP algorithm by using multilayer grids when extracting each path. We obtain coarse and refined estimates of $(x_{n,s}, y_{n,s})$ from a higher- and a lower-layer grid, respectively. Subsequently, $g_{n,s}$ is estimated.

1) Coarse Estimation: The higher-layer grid (denoted by Ξ_{H}) sparsely illustrates the VR of the ULA. Ξ_{H} has the similar expression with (8), but the larger steps are denoted by Δx_{H} and Δy_{H}, satisfying $\Delta x_{\text{H}} \gg \Delta x$ and $\Delta y_{\text{H}} \gg \Delta y$, respectively. In the *s*th iteration, we define $\mathbf{z}_{n,s} \in \mathbb{C}^{M \times 1}$ with the *n*th subvector as $\mathbf{r}_{n,\text{res}}^{(s)}$ and zero elsewhere. We select the grid point in Ξ_{H}, which has the largest radiation power from $\mathbf{z}_{n,s}$, to be the coarse estimate of the coordinate, that is,

$$(\hat{x}_{n,s}, \hat{y}_{n,s}) = \max_{(x,y) \in \Xi_{\text{H}}} \rho_{\{n\}, \mathbf{z}_{n,s} \to (x,y)}. \tag{12}$$

2) Refined Estimation: The lower-layer grid $\Xi_{\text{L}}(\hat{x}_{n,s}, \hat{y}_{n,s})$ densely illustrates a small region around $(\hat{x}_{n,s}, \hat{y}_{n,s})$, where

$$\begin{aligned} \Xi_{\text{L}}(\hat{x}, \hat{y}) = \{(x, y) | \\ x = \hat{x} - \bar{X}, \ldots, \hat{x} - \Delta x, \hat{x}, \hat{x} + \Delta x, \ldots, \hat{x} + \bar{X}; \\ y = \hat{y} - \bar{Y}, \ldots, \hat{y} - \Delta y, \hat{y}, \hat{y} + \Delta y, \ldots, \hat{y} + \bar{Y}\}, \end{aligned} \tag{13}$$

$\bar{X}$ and $\bar{Y}$ set the width and height of the low-layer grid. We search the lower-layer grid to obtain the refined estimates:

$$(\tilde{x}_{n,s}, \tilde{y}_{n,s}) = \max_{(x,y) \in \Xi_{\text{L}}(\hat{x}_{n,s}, \hat{y}_{n,s})} \rho_{\{n\}, \mathbf{z}_{n,s} \to (x,y)}. \tag{14}$$

The attenuation factor of path *s* is estimated by

$$\tilde{g}_{n,s} = g_{\{n\}, \mathbf{z}_{n,s} \to (\tilde{x}_{n,s}, \tilde{y}_{n,s})} \tag{15}$$

where

$$g_{\Phi, \mathbf{z} \to (x,y)} = \frac{(\mathbf{a}(x, y) \odot \mathbf{p}(\Phi))^H \mathbf{z}}{\|\mathbf{a}(x, y) \odot \mathbf{p}(\Phi)\|^2}. \tag{16}$$

3) Stopping Criterion: The iterations terminate when only the noise remains in the residue. By applying the stopping criterion in [11], the refined OMP algorithm can be terminated when

$$\left\| \mathcal{F}\left\{ \mathbf{r}_{n,\text{res}}^{(s)} \right\} \right\|_\infty < \log(M/N) - \log\log\left(1 - (1 - P_{\text{fa}})^{-M/N}\right), \tag{17}$$

where $\mathcal{F}\{\cdot\}$ represents the Fourier transform and P_{fa} is the false alarm rate. The BS finds $\tilde{S}_n$ scatterers that can be seen by subarray *n*. When $\tilde{S}_n > 0$, the channel of subsystem *n* is reconstructed by

$$\tilde{\mathbf{h}}_n = \sum_{s=1}^{\tilde{S}_n} \tilde{g}_{n,s} \mathbf{a}_n(\tilde{x}_{n,s}, \tilde{y}_{n,s}). \tag{18}$$

If $\tilde{S}_n = 0$, then $\tilde{\mathbf{h}}_n = \mathbf{0}$.

The subarray-wise method applies the refined OMP algorithm on $\mathbf{r}_1, \ldots, \mathbf{r}_N$ separately, as illustrated in Alg. 1. The estimation results also reflect the mapping between subarrays and scatterers from the view of the subarrays. For example, if $(\tilde{x}_{1,1}, \tilde{y}_{1,1}) = (\tilde{x}_{2,1}, \tilde{y}_{2,1}) = (x_1, y_1)$, then scatterer 1 sees subarrays 1 and 2 simultaneously. However, the accuracy of $(\tilde{x}_{n,s}, \tilde{y}_{n,s})$ is dependent on the scale of a subarray. If M/N is small, then the accuracy will be greatly affected due to the loss of spatial resolution. Consequently, the BS cannot recognize the two scatterers being the same one. Nevertheless, when the transceiver design on subarray 1 is independent from that on subarray 2, the BS does not need to discover this identity.

Algorithm 1 Subarray-Wise Channel Estimation

Input: $\mathbf{r}_1, \ldots, \mathbf{r}_N$

Output: $\left\{ \tilde{\mathbf{h}}_n, (\tilde{x}_{n,s}, \tilde{y}_{n,s}) \right\}, s = 1, \ldots, \tilde{S}_n, n = 1, \ldots, N$

```
while n = 1, ..., N do
    Set s = 1, and r_{n,res}^{(s)} = r_n.
    while (17) does not hold for subarray n do
        Coarsely estimate (x̂_{n,s}, ŷ_{n,s}) by (12).
        Refine estimate (x̃_{n,s}, ỹ_{n,s}) by (14).
        Estimate g̃_{n,s} by (15).
        Set s = s + 1, and update r_{n,res}^{(s)}.
    end while
    Reconstruct h̃_n.
end while
```

C. Scatterer-Wise Channel Estimation

The method involving the joint manipulation of multiple subarrays is considerably effective in maximizing the array gain and improving the system efficiency. In this condition, the identification of common scatterers in the VRs of different

[3]The sparsity of the near-field channel is shown in the spatial domain. The spatial domain channel is obtained by projecting the antenna domain channel $\mathbf{h}$ to the uniformly sampled *xy*-directions in Ξ as (7).

Algorithm 2 Scatterer-Wise Channel Estimation

Input: $\mathbf{r}_1, \ldots, \mathbf{r}_N$

Output: $\tilde{\mathbf{h}}, \left\{(\tilde{x}_s, \tilde{y}_s), \tilde{\Phi}_s\right\}, s = 1, \ldots, \tilde{S}$

1: Set $s = 1$, and $\mathbf{r}_{\text{res}}^{(s)} = \mathbf{r}$.
2: **while** (17) does not hold for at least one subarray **do**
3: Include subarrays that do not satisfy (17) into $\Phi^{(s)}$.
4: Coarsely estimate $(\hat{x}_s, \hat{y}_s)$ by (20).
5: Coarsely estimate $\hat{\Phi}_s$ by observing (21).
6: Refine estimate $(\tilde{x}_s, \tilde{y}_s)$ by (23).
7: Coarsely estimate $\hat{g}_s$ by (22).
8: Refine estimate $\tilde{\Phi}_s$ by observing (25).
9: Refine estimate $\tilde{g}_s$ by (26).
10: Set $s = s+1$, and update $\mathbf{r}_{\text{res}}^{(s)}$.
11: **end while**
12: Reconstruct $\tilde{\mathbf{h}}$.

subarrays becomes essential. The scatterer-wise method estimates the channel directly from the view of scatterers. As shown in Fig. 2, with more subarrays seeing a scatterer, the directionality of the array pattern becomes more distinct. Thus, the scatterer-wise method is designed to position the scatterer by jointly utilizing all the subarrays that can see the scatterer.

The scatterer-wise method is also based on the refined OMP algorithm, as illustrated in Alg. 2. In the *s*th iteration, we estimate the coordinate of scatterer *s* (i.e., (x_s, y_s)) and the attenuation factor g_s, and determine the subarrays that can see this scatterer (i.e., Φ_s) from the residue

$$\mathbf{r}_{\text{res}}^{(s)} = \mathbf{r} - \sqrt{P}\sum_{i=1}^{s-1} \tilde{g}_i \mathbf{a}(\tilde{x}_i, \tilde{y}_i) \odot \mathbf{p}(\tilde{\Phi}_i), \tag{19}$$

where $\tilde{g}_i$, $(\tilde{x}_i, \tilde{y}_i)$, and $\tilde{\Phi}_i$ are the estimates of g_i, (x_i, y_i), and Φ_i, respectively. At the beginning of the *s*th iteration (Step 3), the subarrays whose residues do not satisfy (17) are included in $\Phi^{(s)}$. If $\Phi^{(s)}$ is empty, then Alg. 2 is terminated. Otherwise, we define $\mathbf{z}^{(s)} \in \mathbb{C}^{M\times 1}$ whose *n*th subvectors is the *n*th subvector of $\mathbf{r}_{\text{res}}^{(s)}$ if $n \in \Phi^{(s)}$; otherwise, the subvector is zero.

1) Coarse Estimation: We calculate $(\hat{x}_s, \hat{y}_s)$, $\hat{\Phi}_s$, and $\hat{g}_s$ at Steps 4, 5, and 7. The coordinate is coarsely estimated by

$$(\hat{x}_s, \hat{y}_s) = \max_{(x,y)\in\Xi_{\text{H}}} \rho_{\Phi^{(s)}, \mathbf{z}^{(s)}\to(x,y)}. \tag{20}$$

Then, we derive $\hat{\Phi}_s$ from $(\hat{x}_s, \hat{y}_s)$. $\hat{\Phi}_s$ is a subset of $\Phi^{(s)}$. The subarrays in $\hat{\Phi}_s$ exhibit the largest radiation power from $\mathbf{z}^{(s)}$ to (x_s, y_s). In Step 5, we calculate the radiation power at each subarray in $\Phi^{(s)}$ and normalize these power values by

$$\gamma_n = \frac{\rho_{\{n\}, \mathbf{z}^{(s)}\to(\hat{x}_s, \hat{y}_s)}}{\sum_{j\in\Phi^{(s)}} \rho_{\{j\}, \mathbf{z}^{(s)}\to(\hat{x}_s, \hat{y}_s)}} \tag{21}$$

where $n \in \Phi^{(s)}$. The sum of the largest $\hat{N}_s$ values of γ_t is assumed to be beyond a threshold δ, where $0 < \delta < 1$. Then, the corresponding $\hat{N}_s$ subarrays are included in $\hat{\Phi}_s$.

We do not estimate $\hat{g}_s$ based on $(\hat{x}_s, \hat{y}_s)$ and $\hat{\Phi}_s$ because the accuracy of $\hat{g}_s$ will be low. Instead, we estimate $\hat{g}_s$ after refining $(\tilde{x}_s, \tilde{y}_s)$. We define $\hat{\mathbf{z}}_s \in \mathbb{C}^{M\times 1}$ whose *n*th subvectors is *n*th subvector of $\mathbf{r}_{\text{res}}^{(s)}$ if $n \in \hat{\Phi}_s$; otherwise, it is zero. $\hat{g}_s$ is calculated by

$$\hat{g}_s = g_{\hat{\Phi}_s, \hat{\mathbf{z}}_s\to(\tilde{x}_s, \tilde{y}_s)}. \tag{22}$$

2) Refined Estimation: We refine the coarse estimates to $(\tilde{x}_s, \tilde{y}_s)$, $\tilde{\Phi}_s$, and $\tilde{g}_s$ at Steps 6, 8, and 9, respectively. The coordinate of scatterer *s* is refined by

TABLE I
COMPUTATIONAL COMPLEXITY

Step	Subarray-wise	Scatterer-wise
Stopping criterion	$O(\sum_{n=1}^{N} \tilde{S}_n \frac{M}{N} \log_2 \frac{M}{N})$	$O(\tilde{S} M \log_2 \frac{M}{N})$
Estimate $(\hat{x}, \hat{y})$	$O(\sum_{n=1}^{N} \tilde{S}_n \lvert\Xi_{\text{H}}\rvert \frac{M}{N})$	$O(\tilde{S} \lvert\Xi_{\text{H}}\rvert M)$
Estimate $\hat{\Phi}$	0	$O(\tilde{S} \lvert\Phi^{(s)}\rvert M)$
Estimate $\hat{g}$	0	$O(\tilde{S} M)$
Estimate $(\tilde{x}, \tilde{y})$	$O(\sum_{n=1}^{N} \tilde{S}_n \lvert\Xi_{\text{L}}\rvert \frac{M}{N})$	$O(\tilde{S} \lvert\Xi_{\text{L}}\rvert M)$
Estimate $\tilde{\Phi}$	0	$O(\tilde{S} \lvert\hat{\Phi}_s\rvert M)$
Estimate $\tilde{g}$	$O(\sum_{n=1}^{N} \tilde{S}_n M)$	$O(\tilde{S} M)$

$$(\tilde{x}_s, \tilde{y}_s) = \max_{(x,y)\in\Xi_{\text{L}}(\hat{x}_s, \hat{y}_s)} \rho_{\hat{\Phi}_s, \hat{\mathbf{z}}_s\to(x,y)}. \tag{23}$$

Then, we estimate $\tilde{\Phi}_s$. Given the directionality of the array pattern, we can derive that subarray $n \in \Phi^{(s)}$ satisfies

$$\mathbb{E}\left[\rho_{\{n\}, \mathbf{z}^{(s)}\to(\tilde{x}_s, \tilde{y}_s)}\right] = \begin{cases} \mathbb{E}\left[\left| g_s \mathbf{b}_n^H(\tilde{x}_s, \tilde{y}_s) \mathbf{a}_n(x_s, y_s)\right|^2 + \|\mathbf{w}_n\|^2\right], & \text{if } n \in \Phi_s, \\ \mathbb{E}\left[\|\mathbf{w}_n\|^2\right], & \text{else,} \end{cases} \tag{24}$$

where $\mathbf{b}_n(x, y)$ is the *n*th subvector of $\mathbf{b}(x, y)$, $\mathbb{E}[\,\cdot\,]$ means taking an expectation, and $\mathbb{E}[\|\mathbf{w}_n\|^2] = M/N$. By applying $(\tilde{x}_s, \tilde{y}_s)$ and $\hat{g}_s$ to (24) and by considering the estimation errors of these parameters, we define that for subarray $n \in \Phi^{(s)}$, if

$$\rho_{\{n\}, \mathbf{z}^{(s)}\to(\tilde{x}_s, \tilde{y}_s)} \geq \alpha \left|\hat{g}_s \mathbf{b}_n^H(\tilde{x}_s, \tilde{y}_s) \mathbf{a}_n(\tilde{x}_s, \tilde{y}_s)\right|^2 + M/N, \tag{25}$$

is satisfied, where $0 < \alpha < 1$, then *n* is included in $\tilde{\Phi}_s$.

We define $\tilde{\mathbf{z}}_s \in \mathbb{C}^{M\times 1}$ whose *n*th subvectors is the *n*th subvector of $\mathbf{r}_{\text{res}}^{(s)}$ if $n \in \tilde{\Phi}_s$; otherwise, it is zero. Then, $\tilde{g}_s$ is calculated by

$$\tilde{g}_s = g_{\tilde{\Phi}_s, \tilde{\mathbf{z}}_s\to(\tilde{x}_s, \tilde{y}_s)}. \tag{26}$$

When Alg. 2 is terminated, we apply $\tilde{g}_s$, $(\tilde{x}_s, \tilde{y}_s)$, and $\tilde{\Phi}_s$ to (5) and obtain the reconstructed channel $\tilde{\mathbf{h}}$.

The complexity of each step in the two methods are compared in Table I, where $|\Xi_{\text{H}}|$, $|\Xi_{\text{L}}|$, $|\Phi^{(s)}|$, $|\hat{\Phi}_s|$, and $|\tilde{\Phi}_s|$ denote the sizes of Ξ_{H}, Ξ_{L}, $\Phi^{(s)}$, $\hat{\Phi}_s$, and $\tilde{\Phi}_s$, respectively. The complexity of the stopping criterion evaluation and that of the parameter estimation are dominated by the DFT transformation and the calculation of the inner products, respectively. Given that $\max(\tilde{S}_n) \leq \tilde{S}$, it satisfies $\sum_{n=1}^{N} \tilde{S}_n/N \leq \tilde{S}$. Moreover, the subarray-wise method does not need to estimate $\hat{\Phi}$, $\hat{g}$, and $\tilde{\Phi}$. Therefore, the complexity of the subarray-wise method is smaller than that of the scatterer-wise method.

The subarray-wise method estimates $\mathbf{h}_n$ simply from $\mathbf{r}_n$. By contrast, the scatterer-wise method estimates $\mathbf{h}_n$ from $\mathbf{r}$, which contains the interference from other subarrays. Thus, the subarray-wise method obtains much more accurate channel estimation results. However, the scatterer-wise method utilizes the multiple subarray gain to estimate the positions and VRs of the scatters, thereby achieving much more accurate positioning and mapping results. Therefore, the subarray-wise method is suitable for the low-complexity subarray-based transceiver design. The scatterer-wise method entails a substantially efficient and comprehensive globalized transceiver design.

IV. NUMERICAL RESULTS

The performances of the proposed channel estimation methods are evaluated. Considering the close distance between the array and the user or last-hop scatterers, we set M = 1,024,

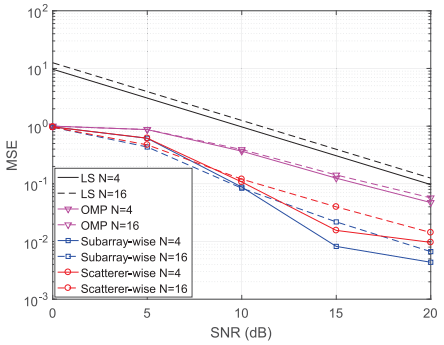

Fig. 3. Comparisons of MSE performances of the proposed methods, LS, and OMP (ignoring non-stationarity).

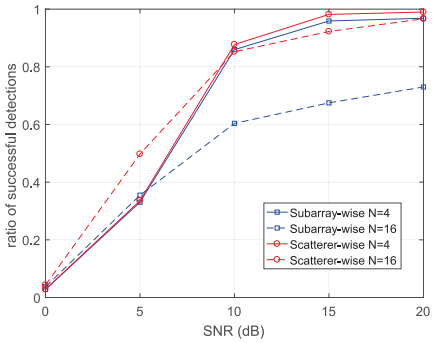

Fig. 4. Ratios of successful detections of the two channel estimation methods under different settings of N.

$d = 1/2$, $X_{\min} = 20$, $X_{\max} = 200$, $Y_{\min} = -600$, and $Y_{\max} = 600$. Following a previous setting of the subarray size in [7], we consider the cases of $N \in \{4, 16\}$. $S = 2$ scatterers are randomly located in the VR of the ULA. $N_s = N/2$ and $0.5 < |g_s|^2 < 1$ hold for $s = 1, \ldots, S$. We set $\Delta x_{\mathrm{H}} = \Delta y_{\mathrm{H}} = 4$, $\Delta x = \Delta y = 0.1$, $P_{\mathrm{fa}} = 0.01$ for the grids, and $\delta = 0.5$, $\alpha = 0.8$ for the scatterer-wise method.

Fig. 3 compares the MSEs of the proposed methods with those of the LS method and evaluates the effectiveness of considering non-stationarity in the channel estimation by comparing it with the case when OMP is directly applied and $N = 1$ is supposed. The linear value of the signal-to-noise ratio (SNR) equals P. We only consider the subarrays of $\Psi_n \neq \emptyset$ and calculate the MSE of the estimated channel $\tilde{\mathbf{h}}_n \in \mathbb{C}^{\frac{M}{N} \times 1}$ as $\mathbb{E}[\|\tilde{\mathbf{h}}_n - \mathbf{h}_n\|^2 / \|\mathbf{h}_n\|^2]$. Notably, ignoring the non-stationarity and simply supposing $N = 1$ will sharply degrade MSE performance. The MSE of the LS method is larger than 10^{-2} at SNR $= 20$ dB because $D_0(x, y)/D_m(x, y) \leq 1$ holds in (1). LS has the drawback of increasing noise. The proposed methods involve considerably lower MSEs and can position the scatterers and determine the non-stationarity, thereby showing great advantage. In the high SNR region, the subarray-wise method, despite its relatively lower complexity, exhibits better MSE performance than the scatterer-wise method, which is in accordance with the analysis in Section III.

Fig. 4 further evaluates the accuracy of the scatterer positioning and non-stationary mapping results of the two methods under the same condition illustrated in Fig. 3. The mapping between subarray n and scatterer s is successfully detected if one detected scatterer t exists, in which its Euclidean distance with (x_s, y_s) is less than 10 (normalized by wavelength), and scatterer t can be seen by subarray n. When the SNR is less than 10 dB, both methods cannot work well. With the increase in SNR, the subarray-wise method can accurately position the scatterers when $N = 4$, that is, the scale of each subarray is large. Moreover, the scatterer-wise method always outperforms the subarray-wise method. Notably, the performance gap between the two methods becomes prominent with the increase in N. This finding can be explained by the accuracy of the refined OMP algorithm, which is degraded due to the reduction of the subarray scale. However, the scatterer-wise method maintains the high positioning and mapping accuracy results with the integrated array gain. When $N = 16$ and SNR ≥ 15 dB, the successful detection ratio of the subarray-wise method exceeds 0.9, demonstrating the effectiveness of the scatterer-wise method.

V. Conclusion

This letter introduced a channel model to describe the near-field non-stationary properties in an extremely large-scale massive MIMO system. Two channel estimation methods were proposed to position the scatterers and identify the mapping between subarrays and scatterers. The subarray-wise method designed for subarray-based transceivers utilized the stationarity on the subarray and positioned the visible scatterers of each subarray. The scatterer-wise method designed for joint subarray transceivers utilized the array gain to position the scatterer while simultaneously determining its mapping with the subarrays. The numerical results demonstrated that the low-complexity subarray-wise method has relatively good MSE performance, whereas the scatterer-wise method can accurately position the scatterers and find almost all the mappings.

References

[1] E. Björnson, L. Sanguinetti, H. Wymeersch, J. Hoydis, and T. L. Marzetta, "Massive MIMO is a reality—What is next? Five promising research directions for antenna arrays," *Digit. Signal Process.*, vol. 94, pp. 3–20, Nov. 2019.

[2] Z. Zhou, X. Gao, J. Fang, and Z. Chen, "Spherical wave channel and analysis for large linear array in LoS conditions," in *Proc. IEEE Globecom Workshops*, San Diego, CA, USA, Dec. 2015, pp. 1–6.

[3] X. Yin, S. Wang, N. Zhang, and B. Ai, "Scatterer localization using large-scale antenna arrays based on a spherical wave-front parametric model," *IEEE Trans. Wireless Commun.*, vol. 16, no. 10, pp. 6543–6556, Oct. 2017.

[4] L. L. Magoarou, A. L. Calvez, and S. Paquelet, "Massive MIMO channel estimation taking into account spherical waves," in *Proc. IEEE Int. Workshop Signal Process. Adv. Wireless Commun. (SPAWC)*, Jul. 2019.

[5] E. D. Carvalho, A. Ali, A. Amiri, M. Angjelichinoski, and R. W. Heath, Jr., "Non-stationarities in extra-large scale massive MIMO," *arXiv preprint arXiv:1903.03085*, Mar. 2019.

[6] A. Ali, E. D. Carvalho, and R. W. Heath, Jr., "Linear receivers in non-stationary massive MIMO channels with visibility regions," *IEEE Wireless Commun. Lett.*, vol. 8, no. 3, pp. 885–888, Jun. 2019.

[7] A. Amiri, M. Angjelichinoski, E. D. Carvalho, and R. W. Heath, Jr., "Extremely large aperture massive MIMO: Low complexity receiver architectures," in *Proc. IEEE Globecom Workshops*, Dec. 2018, pp. 1–6.

[8] X. Cheng, K. Xu, J. Sun, and S. Li, "Adaptive grouping sparse Bayesian learning for channel estimation in non-stationary uplink massive MIMO systems," *IEEE Trans. Wireless Commun.*, vol. 18, no. 8, pp. 4184–4198, Aug. 2019.

[9] S. Lu and Z. Wang, "Training optimization and performance of single cell uplink system with massive-antennas base station," *IEEE Trans. Commun.*, vol. 67, no. 2, pp. 1570–1585, Feb. 2019.

[10] J. A. Tropp and A. C. Gilbert, "Signal recovery from random measurements via orthogonal matching pursuit," *IEEE Trans. Inf. Theory*, vol. 53, no. 12, pp. 4655–4666, Dec. 2007.

[11] B. Mamandipoor, D. Ramasamy, and U. Madhow, "Newtonized orthogonal matching pursuit: Frequency estimation over the continuum," *IEEE Trans. Signal Process.*, vol. 64, no. 19, pp. 5066–5081, Oct. 2016.